 Selected for a Viewpoint in *Physics*

Stopped Light and Image Storage by Electromagnetically Induced Transparency up to the Regime of One Minute

Georg Heinze,[*] Christian Hubrich, and Thomas Halfmann[†]

Institut für Angewandte Physik, Technische Universität Darmstadt, Hochschulstraße 6, 64289 Darmstadt, Germany
(Received 28 March 2013; published 15 July 2013)

The maximal storage duration is an important benchmark for memories. In quantized media, storage times are typically limited due to stochastic interactions with the environment. Also, optical memories based on electromagnetically induced transparency (EIT) suffer strongly from such decoherent effects. External magnetic control fields may reduce decoherence and increase EIT storage times considerably but also lead to complicated multilevel structures. These are hard to prepare perfectly in order to push storage times toward the theoretical limit, i.e., the population lifetime T_1. We present a self-learning evolutionary strategy to efficiently drive an EIT-based memory. By combination of the self-learning loop for optimized optical preparation and improved dynamical decoupling, we extend EIT storage times in a doped solid above 40 s. Moreover, we demonstrate storage of images by EIT for 1 min. These ultralong storage times set a new benchmark for EIT-based memories. The concepts are also applicable to other storage protocols.

Electromagnetically induced transparency (EIT) serves to drive atomic coherences and exploit them in a wide field, ranging from nonlinear optics to quantum information science [1,2]. Among others, the phenomena of slow [3] or stopped light are surely the most stunning EIT effects, which enable EIT-based protocols for quantum memories. The latter have been realized in various media and also on the single photon level [4,5]. Such memories are a key component in optical (quantum) information processing, e.g., in deterministic single photon sources, quantum networks, or quantum repeaters [6]. In particular, the latter define challenging demands with regard to the storage duration in the memory. As an example, the distribution of entanglement over distances of 1000 km requires storage times of milliseconds for multiplexed devices [7,8] or several tens of seconds for standard protocols [9]. However, typical EIT storage times reach only some 100 μs for hot gases [10] or up to one second in ultracold atoms [11,12]. We note that very recently the storage time was extended to 16 s in an ultracold atomic gas [13]. A storage time of roughly 2 s was demonstrated in a rare-earth-ion-doped crystal (REIC) [14]. Although this is still 2 orders of magnitude below the population lifetime T_1 of the REIC, it held the record in EIT-driven memories for several years and attracted considerable attention. The results were often considered as a realistic upper limit for possible storage times, either in EIT or other protocols [15,16].

The long storage times in REICs are due to their unique spectroscopic properties. REICs combine advantages of free atoms (i.e., long coherence times) and solids (i.e., large optical density and scalability). Moreover, data stored in REIC memories do not suffer from atomic diffusion, which strongly limits gas phase memories. As another important feature, we highlight the very long hyperfine population lifetimes in REICs, e.g., $T_1 \sim 100$ s for

$Pr^{3+}:Y_2SiO_5$ [17,18]. However, stochastic magnetic interactions between the dopant ions and the host matrix lead to a reduced coherence time T_2 of ground state hyperfine levels, e.g., $T_2 \approx 500$ μs for $Pr^{3+}:Y_2SiO_5$ [19]. This sets a limit for the storage duration in coherent protocols, e.g., EIT. However, there are possibilities to increase the coherence time in a REIC by an external static magnetic field. The latter reduces the stochastic flipping of nuclear spins in the memory. Moreover, the specific choice of the magnetic field strength in three dimensions (3D) gives rise to hyperfine transitions, which are insensitive to perturbations induced by the host matrix. At such "zero first order Zeeman shift" (ZEFOZ) configurations, the coherence times in $Pr^{3+}:Y_2SiO_5$ were first extended to 860 ms and later to 30 s by additional radio frequency (rf) decoupling pulses [20], although no optical storage protocols were applied in these cases. However, due to a multitude of level splittings in the 3D magnetic field, ZEFOZ leads to a very complicated level structure [compare with Fig. 1(b)]. Without magnetic field, the ground state $^3H_4$ and the optically excited state $^1D_2$ in $Pr^{3+}:Y_2SiO_5$ consist of three doubly degenerate hyperfine levels, with energy gaps in the range of 10 MHz. The optical transition $^3H_4 \leftrightarrow ^1D_2$ is at a wavelength of 606 nm. When a magnetic field is applied, all hyperfine levels shift and split. Taking the large inhomogeneous broadening of the optical transition into account, a monochromatic laser will now drive 36 transitions simultaneously in different frequency ensembles of the inhomogeneous manifold. Probing the generated population distribution results in up to 1296 features in the absorption spectrum. In this mess of frequency ensembles and split levels, it is very hard to determine the perfect conditions (i.e., magnetic field strengths in 3D) for ZEFOZ, as well as an optimal optical preparation sequence (i.e., time profiles of laser intensity and frequency) for EIT.
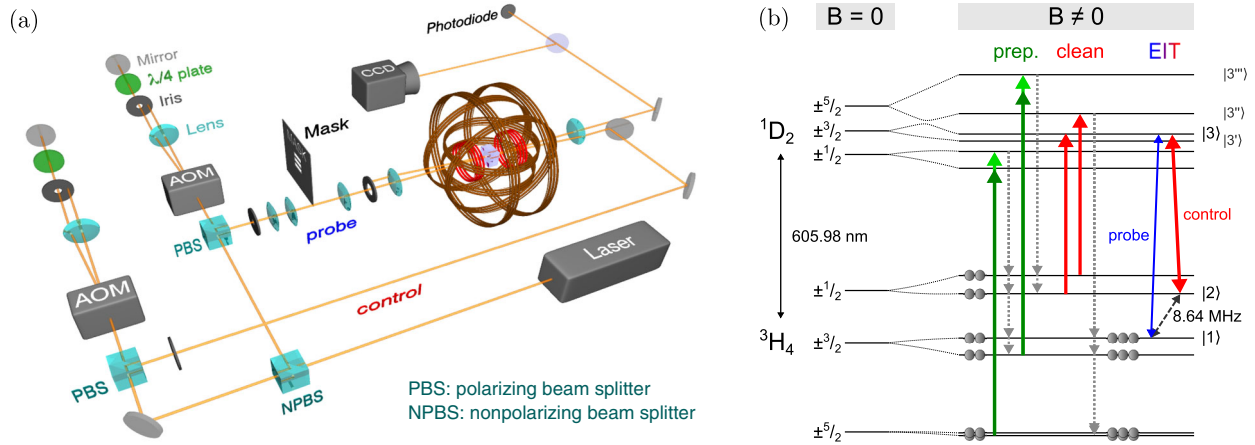
FIG. 1 (color online).   Experimental setup and level scheme in Pr³⁺:Y₂SiO₅. (a) Experimental setup. (b) Energy level diagram of a single ensemble of Pr³⁺ ions, without and with external magnetic field. Green arrows indicate the action of the second step of the preparation pulse sequence (compare with Fig. 2) onto the population distribution in the specific ensemble. Gray, dashed arrows indicate decay processes during optical pumping. Red arrows indicate an additional cleaning pulse.

However, only perfect ZEFOZ conditions and perfect optical preparation sequences permit the EIT storage duration to approach the regime of the population lifetime $T_1 \sim$ 100 s. This requires smart strategies for efficient search and optimization in the large parameter space.

We note that, in principle, it is possible to calculate optimal ZEFOZ conditions from the multilevel Hamiltonian of the crystal [21,22]. However, the calculated field will not be the optimal solution under realistic conditions, e.g., due to perturbing magnetic fields. Even deviations below 1% from the optimal field strongly limit the storage efficiency [20,23]. Even if we assume perfect ZEFOZ, calculation of the optimal intensity and frequency profile in the preparation pulse (also considering pulse propagation effects) remains a barely possible task.

In our Letter, we apply an experimental method to automatically determine the optimal magnetic field for ZEFOZ by gradient search, as well as a self-learning loop with an evolutionary algorithm to automatically find an optimal preparation sequence. The latter method stems from ultrafast laser physics, originally applied to optimize chemical processes on the femtosecond time scale [24]. We combine the concepts with dynamical decoupling strategies to drive storage of light pulses and images by EIT, reaching ultralong storage times up to the regime of one minute, i.e., approaching the population lifetime T_1.

The experimental setup is as follows [see Fig. 1(a)]: The Pr³⁺:Y₂SiO₅ sample (length, 3 mm; doping concentration, 0.05%) is held at cryogenic temperatures below 4 K. Superconducting Helmholtz coils generate the 3D static magnetic field for ZEFOZ. Additional rf coils provide dynamical decoupling sequences. A frequency-stabilized continuous wave dye laser generates optical radiation at 606 nm. The light is split into a weak probe beam line and an intense control beam line, the latter also

providing preparation and cleaning pulses. Acousto-optical modulators (AOMs) control all laser pulses. The preparation and cleaning pulse provide a three-level Λ system with population in the ground state $|1\rangle$, as required for EIT [see Fig. 1(b)]. The probe and control write pulse drive the system into an atomic coherence of hyperfine states $|1\rangle$ and $|2\rangle$. The probe pulse is stored by EIT in the atomic coherence. For retrieval, a control read pulse beats with the atomic coherence to generate a signal beam with identical properties as the probe beam. For detection, a photodiode measures the probe pulse energy and a CCD camera images the probe beam profile. For image storage, we apply a binary mask to imprint transversal image information (e.g., three horizontal stripes) on the probe beam. The images are mapped into the crystal by telescopes in a $4f$ configuration. Hence, we store a spatially confined real image rather than a Fourier image (which would include high space frequencies spreading over a large diameter). This leads to higher storage efficiencies and a much better resolution in the retrieved image.

The experiment starts by estimating the required 3D magnetic field for ZEFOZ from the Hamiltonian. The theoretically obtained value serves as a starting point for an automatic optimization algorithm based on gradient search in the experiment. The algorithm optimizes the 3D magnetic field to obtain long coherence times, which are measured during the optimization process via simple spin echoes. The automatic gradient search algorithm determined an optimal 3D magnetic field $\vec{B}_Z = (741, 177, 215)$ G and a hyperfine transition at 8.64 MHz [Fig. 1(b)] for ZEFOZ. We checked this by recording Raman heterodyne spectra and observed the expected vanishing first order energy shift.

After determination of the ZEFOZ point, we apply the self-learning loop with evolutionary algorithm to optimize
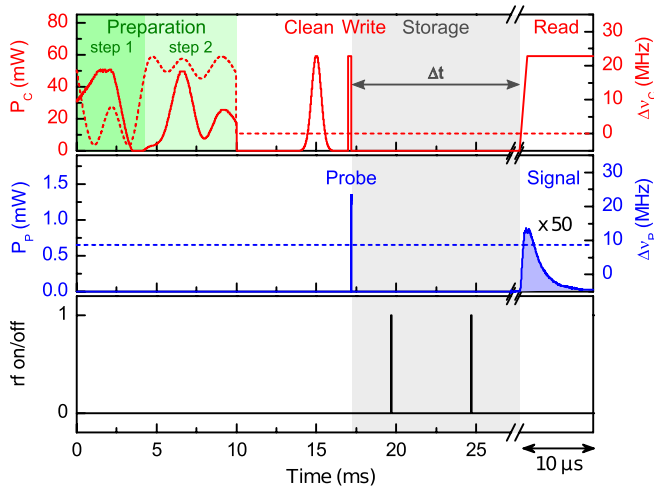
FIG. 2 (color online). Control, probe, and rf pulse sequence in the experiment. The three graphs show power and frequency profiles of the optical control pulse (*C*), optical probe pulse (*P*), and rephasing rf pulses in time. Power profiles (left axis) are drawn as solid lines and frequencies (right axis) as dashed lines. We define all frequencies as detunings relative to the control transition [compare with Fig. 1(b)]. Please note that for better visibility, we interrupted and stretched the time axis during the final retrieval step.
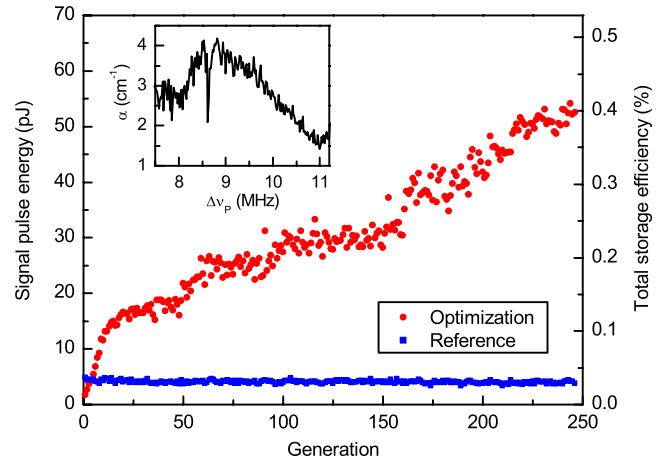

FIG. 3 (color online). Evolution of the self-learning loop toward an optimized preparation pulse. The graph shows the signal pulse energy after light storage (i.e., the "fitness" of the preparation pulses, determined by the evolutionary algorithm) vs the number of generations in the loop. The red dots depict the averaged result of all individuals (i.e., pulses) of a particular generation. The reference (blue squares) corresponds to a single arbitrarily chosen individual of the first generation. The constant reference indicates stable experimental conditions during optimization.

the optical preparation sequence in the complex multilevel scheme. The full experimental pulse sequence consists of five parts (Fig. 2): First, the evolutionary algorithm searches for optimized intensity and frequency profiles in a long preparation pulse. The pulse prepares the dopant ions by a multitude of optical pumping steps to generate optimal conditions for light storage. Second, we apply a cleaning pulse tuned to the frequency of the control transition in EIT. Third, during the EIT write process, a probe and a control pulse drive the atomic coherence [Fig. 1(b)] to store the probe pulse. In a fourth step, we use two rf π pulses to rephase the inhomogeneously broadened coherences [25]. In the fifth step (i.e., the EIT read process), another control pulse beats with the atomic coherence to retrieve the probe pulse, i.e., to generate a signal pulse. The energy of the signal pulse serves as a measure for the quality ("fitness") of light storage.

The self-learning loop with the evolutionary algorithm works as follows: The loop starts with a random set ("generation") of preparation pulses ("genetic individuals"). Each individual is described by a temporal array of intensity and frequency values ("genes"). The self-learning loop applies the pulses for EIT and determines the individuals with the highest fitness, i.e., the best light storage efficiency. The next generation is built by imitating concepts of evolutionary biology: The best individuals are copied into the next generation (cloning). Other good individuals are modified by variations of their genes (mutation) or combination with other fit individuals (inheritance). The loop goes through several hundred

generations, until the gene sequences (i.e., pulse shapes) converge toward an optimum. Figure 3 shows the progress of the self-learning loop, i.e., the increase of signal pulse energy after light storage vs number of completed generations. As expected, the fitness increases monotonically with the generations. The inset shows a clear EIT resonance, as prepared by an individual of the last generation.

The result of the optimization, i.e., the optimal preparation pulse sequence, is plotted in Fig. 2 (upper row). The upper graph shows the control sequence, which consists of four major parts: preparation, cleaning, control write, and control read. The optimized preparation sequence, as determined by the self-learning loop with evolutionary algorithm, is highlighted by a green background. After the cleaning pulse (FWHM duration 700 μs), the medium is ready for light storage. Control write and control read pulses (FWHM duration 200 μs) are separated by the storage duration Δt, as indicated by the gray background. The middle graph shows the initial probe pulse (FWHM duration 10 μs) and the retrieved signal pulse. The lower graph shows the rephasing rf pulses with the example of a single Carr-Purcell rephasing sequence [26]. For long-term storage, the number of rf pulses increases up to 20 000 per second.

The optimized preparation pulse mirrors the complexity of the level scheme at ZEFOZ conditions. Comparison with extended simulations on optical pumping in the inhomogeneously broadened multilevel system, driven by the optimized preparation pulse, yields insight into the population dynamics (which we only briefly summarize here):

In the first step, the preparation frequency varies across a broad range. This creates a region of low absorption within the inhomogeneously broadened medium. In the second step, the frequency varies over a smaller range. This drives several selective pumping processes within specific ensembles. The subsequent cleaning pulse empties state $|2\rangle$ and prepares the system in state $|1\rangle$, as required for EIT. Figure 1(b) gives an example for the action of the preparation pulse in one specific ensemble, which we find to contribute significantly to light storage. However, the simulations show that the optimized preparation pulse also simultaneously prepares three additional ensembles with excited states $|3'\rangle$, $|3''\rangle$, and $|3'''\rangle$ for EIT light storage [see Fig. 1(b)]. This leads to a high absorption coefficient of $\alpha \approx 4$ cm^{-1} on the probe transition (see the inset in Fig. 3).

We note that the storage efficiency of 0.4% in Fig. 3 seems quite low. This is due to technical reasons only: (a) The laser jitter $\Delta\nu_{\text{jitter}} \sim 100$ kHz is larger than the EIT bandwidth $\Gamma_{\text{EIT}} = 35$ kHz, leading to slightly off-resonant storage and readout. (b) EIT suffers from residual signal absorption on other transitions (also in different ensembles of the second magnetic site). (c) The control pulses are not improved by the self-learning loop (to limit optimization times to 1 h). (d) We applied a rather large probe power to operate at saturated EIT. This permits a signal pulse at small intensity fluctuations (as required for a faster optimization loop) but artificially reduces the storage efficiency (which is defined relative to the strong probe pulse). We confirmed experimentally that a simple reduction of probe energy leads to a doubling of the storage efficiency toward 1%.

After the ZEFOZ optimization by gradient search and optimization of the preparation pulse by the evolutionary algorithm, we combined the methods with dynamical decoupling [27,28] to proceed toward long-term light storage. Thus, we replaced the simple rf rephasing sequence of two π pulses by a large number of identical pulse pairs, with a cycling time T_C. Provided the cycling is sufficiently fast, it decouples the Pr^{3+} ions from environmental noise. We improved the rf setup to provide short π pulses with duration of 4 μs. Thus, we fully cover the inhomogeneously broadened hyperfine transition by the bandwidth of the π pulses. This is important for dynamical decoupling to prevent pulse error accumulation.

Figure 4 shows the results of the light storage experiment (i.e., signal pulse energy vs storage time), combining optimized ZEFOZ, optimized preparation sequence, and fast dynamical decoupling for three different cycling times. Obviously, there is no tradeoff between initial storage efficiency and cycling time of the decoupling sequence, as all traces in Fig. 4 start at roughly the same efficiency. The longest storage times are obtained for the fastest cycling with $T_C = 100$ μs, corresponding to 20 000 rf pulses per second. By fitting the data with an exponential decay, we obtain a $1/e$ storage duration of $T_2 = 42.3 \pm 2.6$ s. We
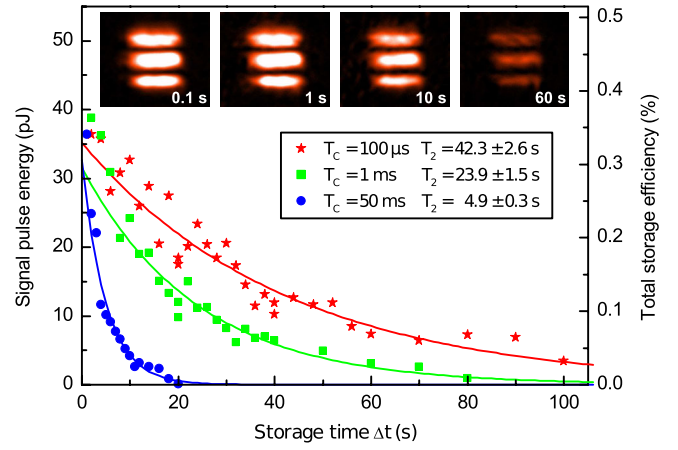

FIG. 4 (color online). Signal pulse energy and retrieved images vs storage time. The three data sets correspond to different cycling times in the dynamical decoupling sequence: $T_C = 100$ μs, $T_C = 1$ ms, and $T_C = 50$ ms. The data are fitted by exponential decays. Dynamical decoupling at the fastest cycling time results in a storage duration of $T_2 = 42.3$ s ($1/e$ time). The insets show the results of image storage and retrieval in the setup, with storage times Δt of 0.1, 1, 10, and 60 s (from left to right). For image storage, we used a decoupling sequence with cycling time $T_C = 100$ μs.

retrieve light pulses up to storage times of well above 1 min. To date, these are the longest storage durations for EIT in any kind of medium.

As a final demonstration, we imprinted images (i.e., three horizontal stripes of length 100 μm) by a binary mask on the probe beam. The EIT protocol also transfers this image information to atomic coherences in the doped crystal. Storage of such complex transversal patterns recently gained considerable attention in the context of high capacity quantum memories [29,30]. The insets in Fig. 4 show images, retrieved for storage durations up to 1 min. The visibility also remains good for ultralong storage times. We note that due to atomic diffusion, storage times of images by EIT in gases are typically limited to 10 μs [31,32]. Our data exceed this by 6 orders of magnitude.

In conclusion, we reported on light storage by EIT in a Pr^{3+}:Y$_2$SiO$_5$ crystal, reaching storage times up to the regime of 1 min. This is achieved by combination of smart optimization strategies in the complex level scheme involving ZEFOZ, self-learning evolutionary algorithms for feedback-controlled pulse shaping, as well as fast and efficient dynamical decoupling. We applied the concepts to store images by EIT for up to 1 min in the doped solid. The investigations serve as a step toward spatially multiplexed quantized memories at ultralong storage durations. Future efforts should aim at single photon storage and application of evolutionary strategies to also support other storage protocols [15,16].

The authors thank D. Schraft and S. Mieth (TU Darmstadt) for experimental support and A. Romanenko

*georg.heinze@physik.tu-darmstadt.de
[†]http://www.iap.tu-darmstadt.de/nlq

[1] M. Fleischhauer, A. Imamoglu, and J. Marangos, Rev. Mod. Phys. **77**, 633 (2005).
[2] J. P. Marangos and T. Halfmann, in *Handbook of Optics*, edited by M. Bass (McGraw-Hill, New York, 2009), 3rd ed., Vol. 4, Chap. 14, p. 14.1.
[3] L. V. Hau, S. E. Harris, Z. Dutton, and C. H. Behroozi, Nature (London) **397**, 594 (1999).
[4] M. D. Eisaman, A. André, F. Massou, M. Fleischhauer, A. S. Zibrov, and M. D. Lukin, Nature (London) **438**, 837 (2005).
[5] T. Chanelière, D. N. Matsukevich, S. D. Jenkins, S.-Y. Lan, T. A. B. Kennedy, and A. Kuzmich, Nature (London) **438**, 833 (2005).
[6] C. Simon, M. Afzelius, J. Appel, A. Boyer de la Giroday, S. J. Dewhurst, N. Gisin, C. Y. Hu, F. Jelezko, S. Kröll, J. H. Müller, J. Nunn, E. S. Polzik, J. G. Rarity, H. De Riedmatten, W. Rosenfeld, A. J. Shields, N. Sköld, R. M. Stevenson, R. Thew, I. A. Walmsley, M. C. Weber, H. Weinfurter, J. Wrachtrup, and R. J. Young, Eur. Phys. J. D **58**, 1 (2010).
[7] O. A. Collins, S. D. Jenkins, A. Kuzmich, and T. A. B. Kennedy, Phys. Rev. Lett. **98**, 060502 (2007).
[8] S.-Y. Lan, A. G. Radnaev, O. A. Collins, D. N. Matsukevich, T. A. Kennedy, and A. Kuzmich, Opt. Express **17**, 13 639 (2009).
[9] N. Sangouard, C. Simon, H. de Riedmatten, and N. Gisin, Rev. Mod. Phys. **83**, 33 (2011).
[10] D. F. Phillips, A. Fleischhauer, A. Mair, R. L. Walsworth, and M. D. Lukin, Phys. Rev. Lett. **86**, 783 (2001).
[11] U. Schnorrberger, J. D. Thompson, S. Trotzky, R. Pugatch, N. Davidson, S. Kuhr, and I. Bloch, Phys. Rev. Lett. **103**, 033003 (2009).
[12] R. Zhang, S. R. Garner, and L. V. Hau, Phys. Rev. Lett. **103**, 233602 (2009).
[13] Y. O. Dudin, L. Li, and A. Kuzmich, Phys. Rev. A **87**, 031801 (2013).
[14] J. J. Longdell, E. Fraval, M. J. Sellars, and N. B. Manson, Phys. Rev. Lett. **95**, 063601 (2005).
[15] W. Tittel, M. Afzelius, T. Chanelière, R. Cone, S. Kröll, S. Moiseev, and M. Sellars, Laser Photonics Rev. **4**, 244 (2010).
[16] M. Afzelius, C. Simon, H. de Riedmatten, and N. Gisin, Phys. Rev. A **79**, 052329 (2009).
[17] K. Holliday, M. Croci, E. Vauthey, and U. P. Wild, Phys. Rev. B **47**, 14 741 (1993).
[18] M. Nilsson, L. Rippe, S. Kröll, R. Klieber, and D. Suter, Phys. Rev. B **70**, 214116 (2004).
[19] B. S. Ham, M. S. Shahriar, M. K. Kim, and P. R. Hemmer, Opt. Lett. **22**, 1849 (1997).
[20] E. Fraval, M. J. Sellars, and J. J. Longdell, Phys. Rev. Lett. **95**, 030506 (2005).
[21] E. Fraval, M. J. Sellars, and J. J. Longdell, Phys. Rev. Lett. **92**, 077601 (2004).
[22] M. Lovrić, P. Glasenapp, and D. Suter, Phys. Rev. B **85**, 014429 (2012).
[23] M. Lovrić, P. Glasenapp, D. Suter, B. Tumino, A. Ferrier, P. Goldner, M. Sabooni, L. Rippe, and S. Kröll, Phys. Rev. B **84**, 104417 (2011).
[24] T. Brixner and G. Gerber, ChemPhysChem **4**, 418 (2003).
[25] G. Heinze, A. Rudolf, F. Beil, and T. Halfmann, Phys. Rev. A **81**, 011401 (2010).
[26] H. Carr and E. Purcell, Phys. Rev. **94**, 630 (1954).
[27] L. Viola, E. Knill, and S. Lloyd, Phys. Rev. Lett. **82**, 2417 (1999).
[28] W. Yang, Z.-Y. Wang, and R.-B. Liu, Front. Phys. **6**, 2 (2011).
[29] D. V. Vasilyev, I. V. Sokolov, and E. S. Polzik, Phys. Rev. A **77**, 020302 (2008).
[30] A. Grodecka-Grad, E. Zeuthen, and A. S. Sørensen, Phys. Rev. Lett. **109**, 133601 (2012).
[31] M. Shuker, O. Firstenberg, R. Pugatch, A. Ron, and N. Davidson, Phys. Rev. Lett. **100**, 223601 (2008).
[32] P. K. Vudyasetu, R. M. Camacho, and J. C. Howell, Phys. Rev. Lett. **100**, 123903 (2008).